Nanoscale

PAPER

View Article Online
View Journal

Cite this: DOI: 10.1039/d4nr03369h

Electrical transport phenomena in two-dimensional metallic 2H-$NbSe_2$: an experimental and theoretical study

Jeongmin Kim,†[a] Seonhye Youn,†[b] Damin Lee,[a,c] Chan Woong Kim,[c] Hongjae Moon,[b] Seok-Hwan Chung,[a] Hoyoung Kim,[c] Dong Hwan Kim,[a] Sumin Kim,[d] Jong Wook Roh,[c] Joonho Bang*[e,f] and Wooyoung Lee*[b]

Received 16th August 2024,
Accepted 23rd October 2024

DOI: 10.1039/d4nr03369h

rsc.li/nanoscale

Two-dimensional (2D) metallic transition metal dichalcogenides (TMDCs) have attracted extensive interest in various fields owing to their unique electronic properties. However, studies on their transport properties and the modulation of these properties based on their band structure are limited. Herein, we studied the transport phenomena in 2D metallic 2H-$NbSe_2$ using experimental and theoretical approaches. The transport properties, including electrical conductivity (σ) and Seebeck coefficient (S), of mechanically exfoliated 2H-$NbSe_2$ nanosheets were measured. We observed field effect-dependent variations in σ and S of the 2H-$NbSe_2$ nanosheets. Theoretical calculations of the electronic band structures and estimations of the transport properties of 2D 2H-$NbSe_2$ crystals were conducted to verify and explain the experimental results. The superconducting transition temperature of the exfoliated $NbSe_2$ nanosheets validated the reliability of the sample preparation procedures and indicated the high quality of the samples. Our findings provide a basis for understanding the electrical properties of metallic TMDCs intended for various applications.

1. Introduction

Two-dimensional (2D) layered materials have garnered considerable attention owing to their unique electronic, optical, and mechanical properties. These materials, such as graphene, hexagonal boron nitride, black phosphorus, and transition metal dichalcogenides (TMDCs), find application in nanoelectronics, biosensors, catalysts, supercapacitors, and energy storage and conversion.[1–4] The unique properties of 2D layered materials can be attributed to their strong in-plane covalent bonding and weak out-of-plane van der Waals bonding, as well as quantum confinement effects.[5–8] In particular, 2D TMDCs, which consist of stacked layers of transition metal atoms sandwiched between chalcogen atoms, have received considerable research attention owing to their tunable structures and properties. These materials can be tuned to behave as semiconductors, semimetals, metals, and superconductors.[9–13] In 2D semiconducting TMDCs, such as MoS_2 and WSe_2, the correlations between transport phenomena and band structure as a function of material thickness, temperature, and applied electric field have been extensively investigated.[14–17] Band engineering based on thickness change and semimetallic transport phenomena have been demonstrated in $PtSe_2$, which has a small overlap between the conduction and valence bands.[18,19] The ability of 2D metallic TMDCs, such as $NbSe_2$, NbS_2, and $TaSe_2$, to simultaneously exhibit two important transition phenomena—charge density wave (CDW) and superconductivity—has made them an ideal candidate for electronic applications.[20,21] In particular, in 2D $NbSe_2$, where the phenomenon of CDW occurs at approximately 33 K and superconducting transition is observed below 7 K, extensive studies related to both phenomena have been reported.[22,23] However, except for studies on these phenomena in the cryogenic temperature range, reports on the transport properties of the metallic TMDCs and their modulation based on the band structure are still limited owing to the high band overlap and carrier density.[24–26]

In this study, we investigated the transport phenomena in metallic 2D 2H-$NbSe_2$ using experimental and theoretical

[a]Division of Nanotechnology, DGIST, 333 Techno Jungang-daero, Hyeonpung-eup, Dalseong-gun, Daegu 42988, Republic of Korea
[b]Department of Materials Science and Engineering, Yonsei University, 50 Yonsei-ro, Seodaemoon-gu, Seoul, 03722, Republic of Korea. E-mail: wooyoung@yonsei.ac.kr
[c]School of Nano Materials Engineering, Kyungpook National University, Gyeongsangbuk-do 37224, Republic of Korea
[d]Department of Magnetic Materials, Korea Institute of Materials Science, Changwon 51508, South Korea
[e]School of Materials Science and Engineering, Gyeongsang National University, Jinju 52828, South Korea. E-mail: bang@gnu.ac.kr
[f]Department of Materials Engineering and Convergence Technology, Gyeongsang National University, Jinju 52828, South Korea
†These authors contributed equally to this work.

approaches. The transport properties, including electrical conductivity (σ) and Seebeck coefficient (S), of mechanically exfoliated 2H-$NbSe_2$ nanosheets of varying thicknesses were measured at different temperatures. We observed field effect-dependent σ and S in the 2H-$NbSe_2$ nanosheets. To verify and explain the experimental results, we theoretically calculated the electronic band structures and transport properties of 2D 2H-$NbSe_2$ crystals with varying layer numbers. To validate the reliability of the sample preparation procedures, including exfoliation and device fabrication, we investigated the crystal and stacking structures of the obtained 2H-$NbSe_2$ nanosheets and confirmed the superconducting transition. The feasibility of the modulation of transport properties of metallic 2H-$NbSe_2$ based on variations in the band structure was demonstrated, affording valuable insights into the electrical properties of metallic TMDCs for a wide range of applications.

2. Experimental methods

Device fabrication

$NbSe_2$ nanosheets were mechanically exfoliated from bulk $NbSe_2$ crystals (HQ Graphene) using the scotch-tape method and transferred onto a heavily doped p^{++} Si substrate with 300 nm-thick SiO_2. Atomic-resolution images were taken by a scanning transmission electron microscope (STEM; JEM-ARM 200F, JEOL) to confirm the crystal structure of the exfoliated $NbSe_2$ nanosheets. Cross-sectional samples for investigating the atomic arrangement were prepared from vertically sliced $NbSe_2$ nanosheets using a dual-beam focused ion beam (FIB; crossbeam 540, ZEISS). Before microdevice fabrication, the thickness of the $NbSe_2$ nanosheets was determined using atomic force microscopy (AFM; XE-150, Park Systems) in contact mode. For transport measurements, the electrodes of the microdevice were patterned using an electron-beam lithography system (VEGA3, Tescan and NPGS, JC Nabity Lithography Systems). Ar plasma treatment (ICP-RIE System, LAT) was conducted on the contact interface between the $NbSe_2$ nanosheet and electrodes before metallization. For electrical and mechanical contacts, Cr (5 nm)/Au (100 nm) electrodes were deposited using a custom-made sputtering system. The sputtering was performed in an Ar atmosphere under a pressure of 2 mTorr at a DC power of 30 W; the deposition rates for Cr and Au were 0.207 and 0.686 nm s^{-1}, respectively. Details of the device fabrication are described in previous reports.[27,28]

Transport measurements

All transport measurements were conducted in high vacuum ($<5 \times 10^{-6}$ Torr). The resistance values of the $NbSe_2$ nanosheets were determined by measuring the current–voltage (I–V) characteristics with a current source (Keithley Model 6221) and voltmeter (Keithley Model 2182). The voltage difference during Joule heating was measured using a voltmeter (Keithley Model 2182). The temperature difference caused by Joule heating was determined using a lock-in amplifier (SR850, Stanford Research Systems) based on the temperature coefficient of resistance (TCR) method. The temperature-dependence of transport properties was determined using a cryostat measurement chamber (X-1AL, Advanced Research Systems) and physical property measurement system (PPMS, Quantum Design). Detailed methods for obtaining σ and S are described in the results and discussion.

Theoretical calculations

The electronic band structures and transport properties of the $NbSe_2$ nanosheets were theoretically determined *via* first-principle density functional theory (DFT) and Boltzmann transport equation (BTE). The calculations were performed using the generalized gradient approximation (GGA) with the Perdew–Burke–Ernzerhof functional and projector augmented plane wave method implemented in the Vienna *Ab initio* Simulation Program (VASP) code.[29–31] The cut-off energy of the plane-wave basis was set to 600 eV, and a k-point mesh of $12 \times 12 \times 3$ was used. The structural optimizations were performed until the Hellmann–Feynman forces were less than 10^{-3} eV $Å^{-1}$. The transport properties were determined using the Shankland–Koelling–Wood interpolation as implemented in the BoltzTraP2 code.[32,33] The band structures obtained from DFT calculations were interpolated using the extended Shankland algorithm, and the Onsager transport coefficients were determined using the linearized Boltzmann transport equation based on the rigid-band approximation.[34–36]

3. Results and discussion

Structural characterizations

Fig. 1 presents the structural characterization results of the 2H-$NbSe_2$ nanosheets. A monolayer of $NbSe_2$ has a hexagonal lattice structure and comprises three atomic sublayers, in which Nb atoms are sandwiched between Se atoms (Fig. 1(a)).[37] Each Nb atom is coordinated by six Se atoms in a trigonal prismatic geometry with strong intra-layer covalent bonds.[38] Multilayered bulk 2H-$NbSe_2$, which belongs to the $P63/mmc$ space group, is formed by weak inter-layer van der Waal bonds with an AB′ double-layer stacking order (Fig. 1(b)).[28,39]

The top-view high-resolution STEM (HR-STEM) image of the 2H-$NbSe_2$ nanosheet is in good agreement with the expected atomic arrangement of AB′ stacking (Fig. 1(c)). In the dark-field image presented in Fig. 1(c), the Nb atoms appear brighter than the Se atoms. The image presented as an inset to Fig. 1(c), obtained after contrast adjustment, clearly reveals two distinct atomic positions that are consistent with the simulated image in a previous study.[40] The cross-sectional STEM images (Fig. 1(d) and (e)) clearly show the AB′ stacking order between the Se–Nb–Se sandwich structures present in 2H-$NbSe_2$ nanosheets. The lattice constants of a 2H-$NbSe_2$ nanosheet are determined as $a = b = 3.5$ Å and $c = 12.6$ Å. The obtained lattice constants are consistent with previously reported values.[39,41]

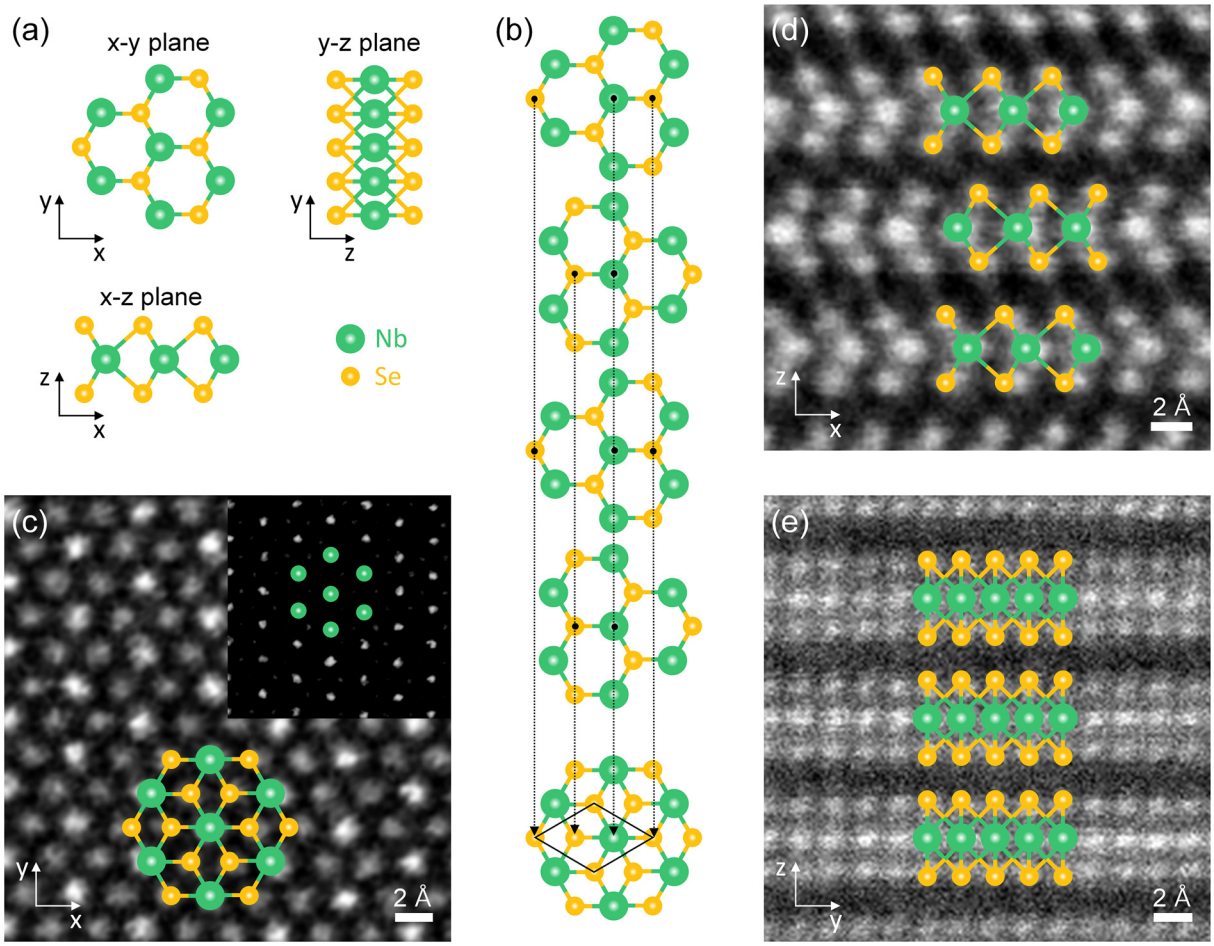

Fig. 1 (a) Top- and side-views of the crystal structures of a monolayer of 2H-$NbSe_2$. (b) Schematic showing stacking order and top-view of a multilayer 2H-$NbSe_2$. (c) Top-view HR-STEM image (*xy*-plane) of a mechanically exfoliated 2H-$NbSe_2$ nanosheet. The inset shows the position of Nb atoms obtained by contrast adjustment. Cross-sectional HR-STEM images of (d) *xz*- and (e) *yz*-planes obtained from vertically sliced 2H-$NbSe_2$ nanosheets. STEM images of *xy*- and *xz*-planes are partially excerpted and redrawn from a previous work with permission.[28]

Transport properties

Fig. 2 presents an image of the microdevice and raw data for determining the transport properties of the 2H-$NbSe_2$ nanosheets. The microdevice comprises a heater electrode and two thermometers (TMs) (Fig. 2(a)). The Seebeck voltage (ΔV_S) was obtained by measuring the voltage difference between the near and far TMs after varying the temperature gradient using the heater. Joule heating is proportional to the square of the heater voltage (V_H); hence, ΔV_S exhibits a parabolic dependence on V_H (Fig. 2(b)). The *I*–*V* measurement was also performed using the same electrodes (inset of Fig. 2(b)). The temperature difference (ΔT) between the two TMs was determined using the relationship between resistance and temperature. The value of ΔT was derived by measuring the resistance of each TM, and the value of S was calculated according to the relation: $S = -\Delta V_S/\Delta T$. The variation in resistance of TM due to Joule heating was determined by measuring the voltage signal (V_{TM}) using the four-terminal technique under a constant current source. The variation of V_{TM} as a function of V_H is also parabolic, similar to that of ΔV_S (Fig. 2(c)). To determine the temperatures using resistance values, the TCR of each TM was obtained by measuring the temperature dependence of V_{TM} (Fig. 2(d)). The obtained values of ΔT also exhibit a parabolic dependence on V_H (inset of Fig. 2(d)). The σ of the nanosheet was calculated using the slope of the *I*–*V* curve and the relation $\sigma = L/Rwt$, where L, R, w, and t are the channel length, resistance, width, and thickness, respectively.[42] The contact resistance between the nanosheet and electrodes was determined to be negligible compared to the resistance of the nanosheet.

Fig. 3 shows the transport properties of the 2H-$NbSe_2$ nanosheets. The temperature dependence of σ was measured using five different nanosheets of different thicknesses ranging from 4.3 to 8.8 nm (Fig. 3(a)). Irrespective of the thickness of the 2H-$NbSe_2$ nanosheets, σ increases with decreasing temperature. The value of σ increases monotonically with decreasing temperature up to 30 K, as observed for the 8.8 and 8.3 nm-thick 2H-$NbSe_2$ nanosheets. The obtained results are consistent with the previously reported metallic characteristics of the 2H-$NbSe_2$ nanosheets, indicating that the dependence

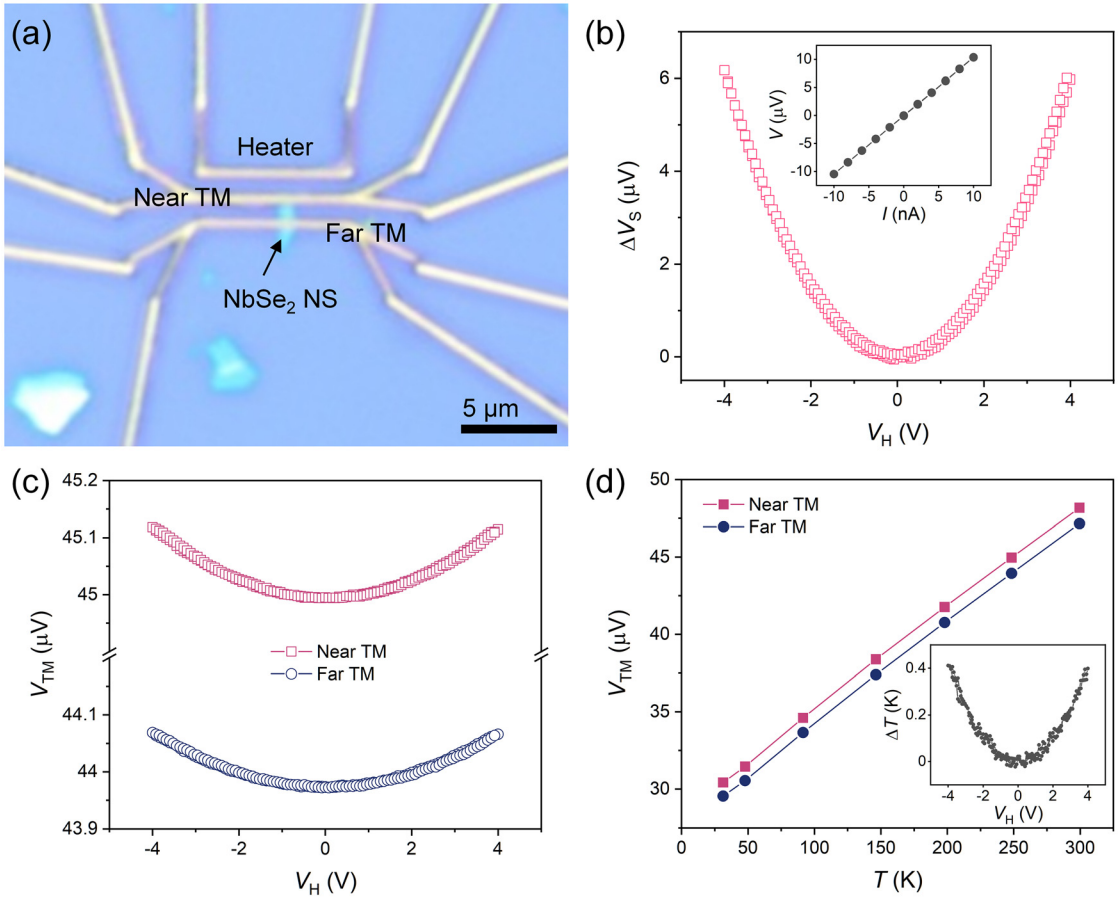

Fig. 2 (a) Optical microscope image of the microdevice based on the 2H-$NbSe_2$ nanosheet. (b) Seebeck voltage as a function of the heater voltage. The inset presents the *I*–*V* curve for resistance determination. (c) Thermometer voltage as a function of the heater voltage. (d) Thermometer voltage as a function of temperature for TCR measurement. The inset shows the temperature difference obtained from the thermometer voltage using the TCR method.

of σ on the carrier mobility is dominant compared to that on the carrier density at different temperatures.[28,43] As shown in the inset of Fig. 3(a), the value of σ decreases as the thickness of the nanosheet decreases, except for the 6.9 nm-thick nanosheet. In general, a decrease in σ due to spatial restrictions is attributed to the reduction in carrier mobility; however, it has been reported that the mobilities of bulk and few-layered 2H-$NbSe_2$ are not significantly different.[43–45] Therefore, it is necessary to analyze the band structures, which are discussed in detail in the theoretical calculation section. The temperature dependence of S of the 2H-$NbSe_2$ nanosheets is presented in Fig. 3(b). The 2H-$NbSe_2$ nanosheets exhibit negative S values at 300 K, and the absolute values of S decrease as the temperature decreases. For the 8.8 and 8.3 nm-thick nanosheets, a negative to positive crossover of S is observed below 100 K. The temperature dependence of S is consistent with that in previous studies on bulk and few-layered 2H-$NbSe_2$.[43] The thickness dependence of S at room temperature, presented in the inset of Fig. 3(b), is discussed with the theoretical results in the next section. The deviation observed in the case of the 6.9 nm-thick nanosheet with regard to the thickness dependence of σ is attributable to a slight change in carrier density, as inferred from its Seebeck coefficient.[18]

To quantitatively understand the transport properties of the 2H-$NbSe_2$ nanosheets, the field effect dependences of σ and S were investigated using the back-gate configuration of the microdevice; the results are presented in Fig. 3(c) and (d). We previously reported that the changes in σ and S caused by the gate modulation of the devices fabricated using metallic 2H-$NbSe_2$ are imperceptible compared to the changes caused by temperature variation.[28] However, reproducible slope of data are obtained from the gate-modulated devices, despite the weak dependence of σ and S on gate modulation and high signal-to-noise ratio of slope. Moreover, a discernible trend is derived by comparing the normalized slopes of σ and S after gate modulation of the devices containing 2H-$NbSe_2$ nanosheets of different thicknesses. The slope of σ, normalized to the value at zero-gate voltage, *versus* the gate voltage is positive irrespective of the thickness of the nanosheet, indicating that the majority of carriers are electrons (Fig. 3(c)).[19,46] The values of normalized slope of σ increase with decreasing

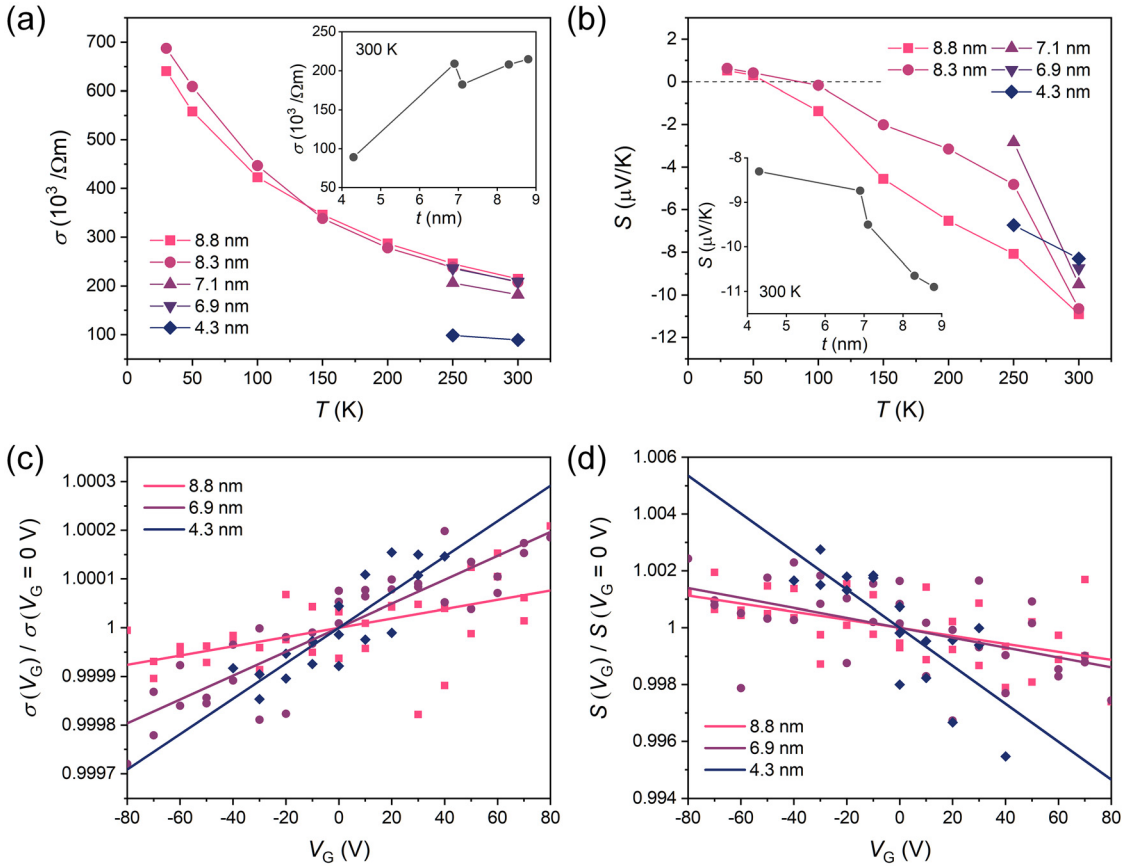

Fig. 3 Temperature-dependent (a) electrical conductivity and (b) Seebeck coefficient of 2H-$NbSe_2$ nanosheets having a thickness of 8.8, 8.3, 7.1, 6.9, and 4.3 nm. The insets to (a) and (b) present the thickness dependences of electrical conductivity and Seebeck coefficient at 300 K, respectively. The error bars are smaller than the symbol sizes for the both electrical conductivity and Seebeck coefficient measurements. Gate-dependent (c) normalized electrical conductivity and (d) normalized Seebeck coefficient of 2H-$NbSe_2$ nanosheets having a thickness of 8.8, 6.9, and 4.3 nm. Data for the 8.8 nm nanosheet were obtained from a previous work with permission.[28]

nanosheet thickness. Based on the reported carrier mobility of 2H-$NbSe_2$, the carrier density of the 8.8 nm-thick nanosheet was found to be approximately 4×10^{21} cm^{-3} and a doping level of 10^{18} cm^{-3} was estimated at the 80 V gate voltage; this is in good agreement with the calculation using the Si–SiO_2–$NbSe_2$ capacitance structure, considering the screening effect.[43,47] A similar gate voltage dependence is observed for the S values. The slopes of normalized values of S as a function of V_G are negative, and the magnitudes of slope value increase with decreasing nanosheet thickness (Fig. 3(d)). In general, when compared to σ, S is more sensitive to carrier density; therefore, as a function of gate voltage, the magnitudes of slope value of normalized S are approximately one order of magnitude higher than those of σ.[48] A higher dependency on the gate voltage, observed after thickness reduction of the nanosheet, may be associated with changes in the band structures. However, the screening effect during gate modulation cannot be ruled out.[49,50] Therefore, to clarify the thickness dependence of the transport phenomenon, theoretical calculations are performed based on band structure.

Theoretical calculations

Fig. 4 shows the electronic band structures and density of states (DOS) for 2H-$NbSe_2$ of different thicknesses. In bulk crystal, the conduction bands cross the Fermi energy level (E_F) and DOS, indicating that the partially filled electronic states mainly originate from Nb with a minor contribution of Se (Fig. 4(a)).[51] Conversely, the DOS of valence bands is mainly driven by Se. The electronic band structures indicate metallic features; this observation is consistent with our experimental observations and previous studies.[52–55] To investigate the change in electronic states as a function of the thickness of 2H-$NbSe_2$, the band structure and DOS of tri-, bi-, and monolayered nanosheets were calculated (Fig. 4(b)–(d)). As the number of layers decreases, the valence bands are further lowered due to the reduced interlayer interactions, resulting in the formation of a band gap. However, no significant changes in the partially occupied conduction bands, which govern the transport phenomena, can be observed.[56] Therefore, the transport properties, including σ and S, were calculated based on the band structures for a more precise understanding.

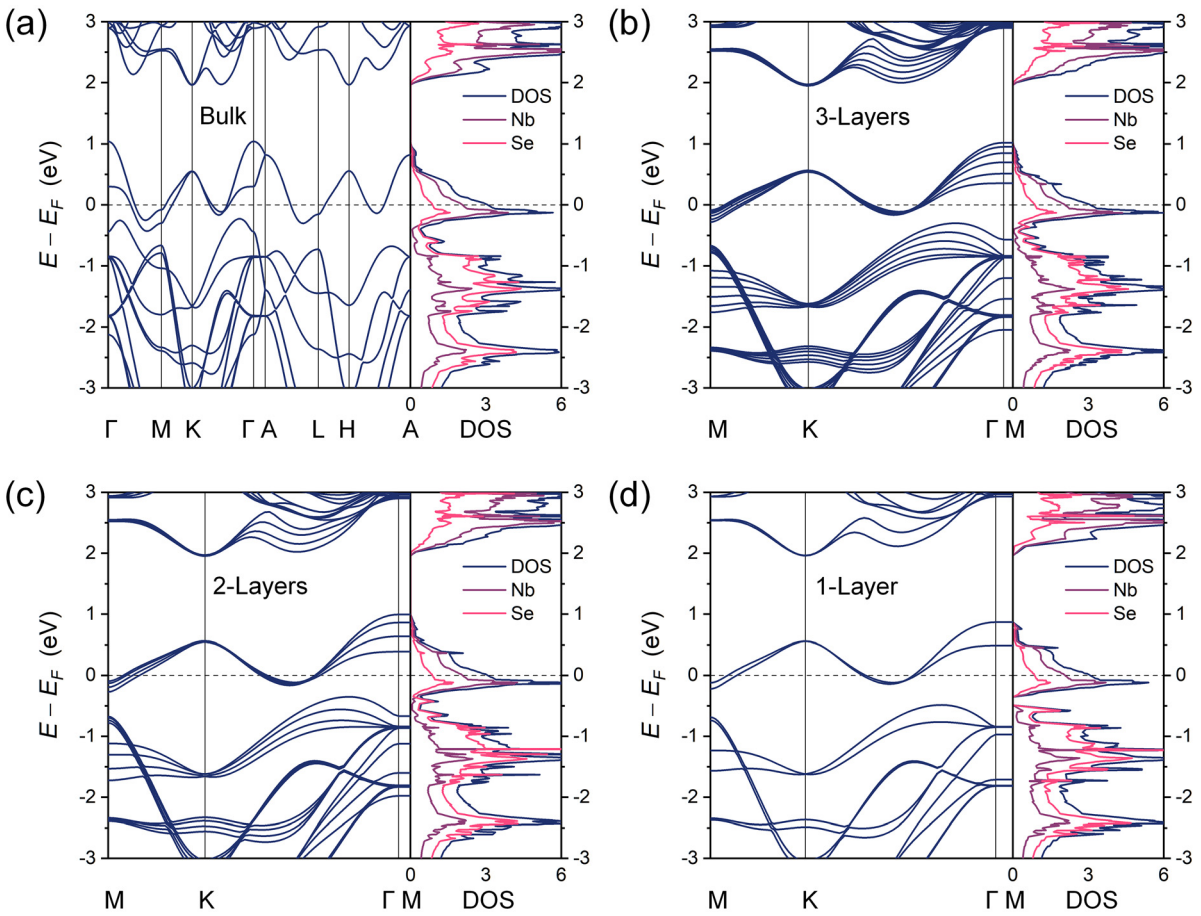

Fig. 4 Electronic band structures and density of states (DOS) of (a) bulk, (b) tri-layered, (c) bi-layered, and (d) mono-layered 2H-$NbSe_2$. Data for bulk 2H-$NbSe_2$ are redrawn from a previous work with permission.[28] The DOS is represented in units of states per formula unit per electronvolt (states f.u.$^{-1}$ eV^{-1}).

Fig. 5 shows the calculated values of σ with respect to scattering time (σ/τ) and S for 2H-$NbSe_2$ of different thicknesses. The obtained values of σ/τ near E_F indicate changes in the band structures and DOS (Fig. 5(a)). This, in turn, indicates that the metallic-type temperature dependence of σ is due to the variation in carrier mobility (Fig. 3). The calculated values of S vary from positive to negative depending on the energy (Fig. 5(b)), because the sign of S reflects the change in DOS for the energy (Fig. 4).[57] Negative S values and temperature variation of these values are observed in the energy range between −0.5 and 0 eV, and the negative to positive crossover of S occurs at low temperatures near the energy values of −0.1 eV (inset of Fig. 5(b)). Further, the dependence of the transport properties on the gate voltage enabled the estimation of the zero-gate E_F of the 2H-$NbSe_2$ nanosheets. The σ and absolute S values exhibit positive and negative dependences on the gate voltage, respectively (Fig. 3(c) and (d)). These experimental results are in good agreement with variations of σ and S obtained using theoretical calculations below 0 eV (Fig. 5(a) and (b)). Furthermore, in this energy range (<0 eV), the change of calculated S according to temperature is consistent with the measured temperature dependence of S.

Next, the effect of changes in the band structure on the transport properties was evaluated by varying the number of layers of 2H-$NbSe_2$. The value of σ/τ decreases as the number of layers decreases, except in the energy range from −0.5 to −0.25 eV (Fig. 5(c)). A monotonic decrease in σ/τ is observed below 0 eV, indicating that the thickness-dependence of σ is linked to the changes in the band structure. The thickness dependence of S could not be clearly determined; however, clearly, the variations in S values caused by the changes in the band structure are more pronounced than the variations in σ (Fig. 5(d)). Furthermore, the energy at which the negative to positive crossover of S occurs decreases with decreasing number of layers, suggesting that the band structure influences the crossover temperature. This explains the changes in the crossover temperature observed in previous studies.[28,43,58]

Superconductivity results

The superconducting property of the exfoliated $NbSe_2$ nanosheet was measured to verify its quality. Fig. 6 shows the temperature-dependent resistivity (ρ) of the nanosheet for temperatures ranging from 2 to 300 K. To achieve sufficient sample length and apply the four-terminal technique, a

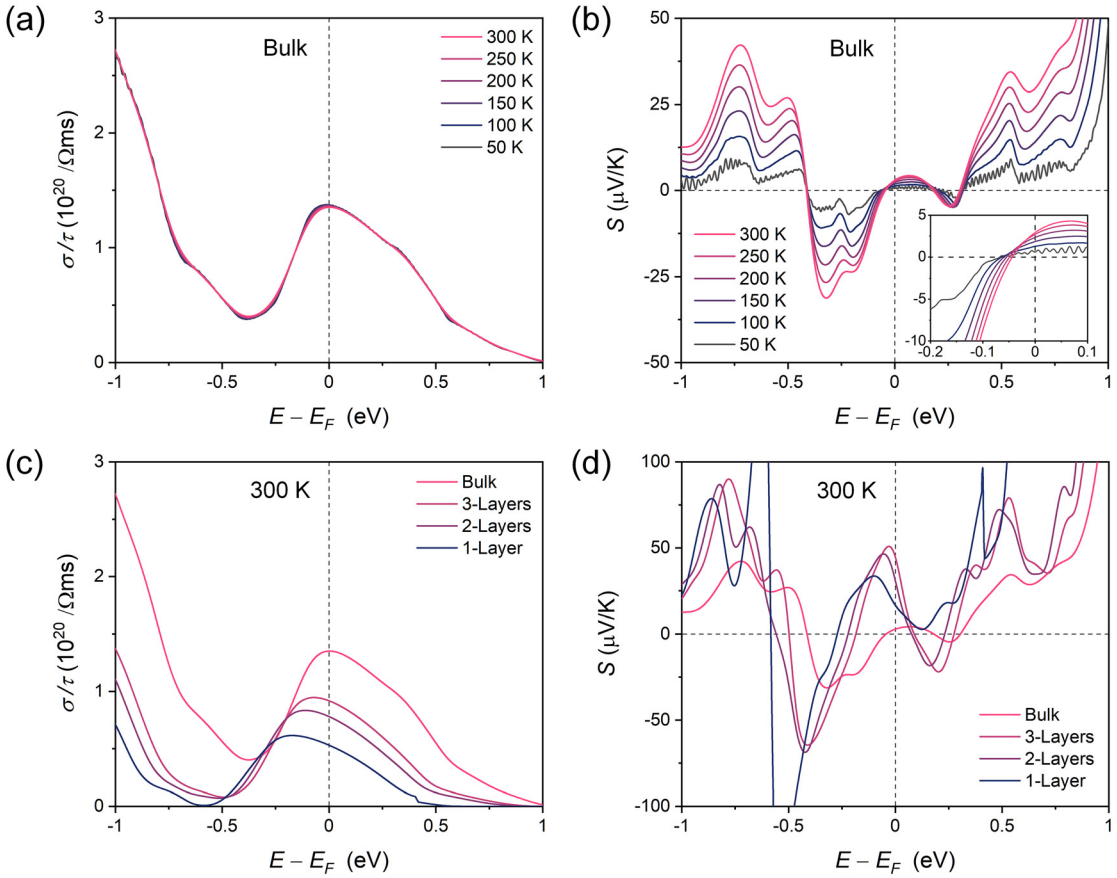

Fig. 5 Theoretically calculated (a) electrical conductivity with respect to scattering time and (b) Seebeck coefficient of bulk 2H-$NbSe_2$ at different temperatures. The inset presents a (b) magnified view of the calculated Seebeck coefficient. The calculated (c) electrical conductivity with respect to scattering time and (d) Seebeck coefficient for bulk, tri-layered, bi-layered, and mono-layered 2H-$NbSe_2$ at 300 K.

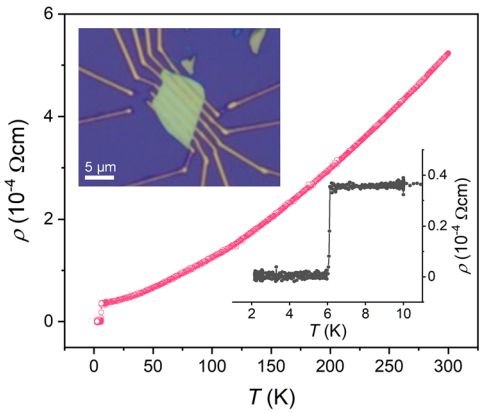

Fig. 6 Temperature-dependent resistivity of a 38.9 nm-thick 2H-$NbSe_2$ nanosheet. The top-left inset shows the microdevice with four-terminal configuration. The bottom-right inset presents a magnified view of the superconducting transition.

38.9 nm-thick nanosheet was used (top-left inset of Fig. 6). The temperature dependence of ρ indicates the metallic characteristic of the nanosheet. The residual resistivity ratio (RRR), defined as $\rho_{300\ K}/\rho_{7\ K}$, is determined to be 14.7. A relatively high RRR indicates that the samples are of high quality; the determined RRR is consistent with the previously reported value obtained using the same source material.[59] However, the RRR was not sufficient to clearly observe the CDW phenomenon around 30 K in the temperature dependence of ρ; the CDW was observed in samples with RRR higher than 20 in previous studies.[60–64] The superconducting transition temperature (T_c) is observed to be 6.3 K (bottom-right inset of Fig. 6). The T_c of 2D $NbSe_2$ gradually decreases from that of bulk $NbSe_2$ (7.2 K) as the sample thickness decreases because of the reduction in carrier density with decreasing number of layers, which reduces electron screening and increases Coulomb interaction.[65–69] Although no distinct CDW phenomenon is observed, the obtained T_c value is consistent with the reported values based on the thickness; this validates the reliability of the sample preparation procedures, including nanosheet exfoliation and device fabrication.

4. Conclusion

In summary, the transport phenomena in 2D 2H-$NbSe_2$ were investigated using experimental and theoretical methods. The

dependence of σ and S of mechanically exfoliated 2H-$NbSe_2$ nanosheets on the temperature, thickness, and gate voltage was measured. The band structures and DOS for 2H-$NbSe_2$ crystals having different number of layers were obtained using first-principle DFT calculations. The σ and S of 2H-$NbSe_2$ crystals were estimated by solving the BTE based on the DFT calculations. Theoretical calculations revealed a metallic-type temperature dependence of σ and negative to positive crossover of S with temperature. The observed thickness dependences of σ and S were correlated with the changes in band structures calculated by varying the number of layers of 2H-$NbSe_2$. The results obtained after gate modulation of devices fabricated using exfoliated 2H-$NbSe_2$ nanosheets were also explained by the variation in energy levels in the calculated band structures, which was used to estimate the E_F of the nanosheets. The use of experimental and theoretical approaches to investigate the transport properties of metallic 2D 2H-$NbSe_2$, including modulation of transport properties based on band engineering, advances the understanding of the electrical properties of metallic TMDCs for diverse applications.

Data availability

The corresponding author can also provide additional data upon reasonable request.

Conflicts of interest

There are no conflicts to declare.

Acknowledgements

This work was supported by the Technology Innovation Program('20013621', Center for Super Critical Material Industrial Technology) funded By the Ministry of Trade, Industry & Energy (MOTIE, Korea), and the Basic Science Research Program through the National Research Foundation of Korea (NRF) funded by the Ministry of Education (NRF-2019R1A6A1A11055660). J. K. acknowledges support from the National Research Foundation of Korea (RS-2023-00211034 and NRF-2021R1A5A8033165). This work was also supported by the fund of Research Promotion Program, Gyeongsang National University, 2022.

References

1 J. Dai, M. Li and X. C. Zeng, Group IVB transition metal trichalcogenides: a new class of 2D layered materials beyond graphene, *Wiley Interdiscip. Rev.: Comput. Mol. Sci.*, 2016, **6**, 211–222.
2 X. Kong, Q. Liu, C. Zhang, Z. Peng and Q. Chen, Elemental two-dimensional nanosheets beyond graphene, *Chem. Soc. Rev.*, 2017, **46**, 2127–2157.
3 S. S. Varghese, S. H. Varghese, S. Swaminathan, K. K. Singh and V. Mittal, Two-dimensional materials for sensing: graphene and beyond, *Electronics*, 2015, **4**, 651–687.
4 S. Mao, J. Chang, H. Pu, G. Lu, Q. He, H. Zhang and J. Chen, Two-dimensional nanomaterial-based field-effect transistors for chemical and biological sensing, *Chem. Soc. Rev.*, 2017, **46**, 6872–6904.
5 K. Choudhary and F. Tavazza, Predicting anomalous quantum confinement effect in van der Waals materials, *Phys. Rev. Mater.*, 2021, **5**, 054602.
6 S.-L. Li, K. Komatsu, S. Nakaharai, Y.-F. Lin, M. Yamamoto, X. Duan and K. Tsukagoshi, Thickness scaling effect on interfacial barrier and electrical contact to two-dimensional MoS2 layers, *ACS Nano*, 2014, **8**, 12836–12842.
7 Z. Gan, L. Liu, H. Wu, Y. Hao, Y. Shan, X. Wu and P. K. Chu, Quantum confinement effects across two-dimensional planes in MoS2 quantum dots, *Appl. Phys. Lett.*, 2015, **106**, 233113.
8 P. Ajayan, P. Kim and K. Banerjee, Two-dimensional van der Waals materials, *Phys. Today*, 2016, **69**, 38–44.
9 Z. Liu, S. Y. Tee, G. Guan and M.-Y. Han, Atomically substitutional engineering of transition metal dichalcogenide layers for enhancing tailored properties and superior applications, *Nano-Micro Lett.*, 2024, **16**, 95.
10 M. Chhowalla, H. S. Shin, G. Eda, L.-J. Li, K. P. Loh and H. Zhang, The chemistry of two-dimensional layered transition metal dichalcogenide nanosheets, *Nat. Chem.*, 2013, **5**, 263–275.
11 Q. H. Wang, K. Kalantar-Zadeh, A. Kis, J. N. Coleman and M. S. Strano, Electronics and optoelectronics of two-dimensional transition metal dichalcogenides, *Nat. Nanotechnol.*, 2012, **7**, 699–712.
12 Z. Wang, C.-Y. Cheon, M. Tripathi, G. M. Marega, Y. Zhao, H. G. Ji, M. Macha, A. Radenovic and A. Kis, Superconducting 2D NbS2 grown epitaxially by chemical vapor deposition, *ACS Nano*, 2021, **15**, 18403–18410.
13 Z. Huang, W. Zhang and W. Zhang, Computational search for two-dimensional MX2 semiconductors with possible high electron mobility at room temperature, *Materials*, 2016, **9**, 716.
14 A. Ciarrocchi, A. Avsar, D. Ovchinnikov and A. Kis, Thickness-modulated metal-to-semiconductor transformation in a transition metal dichalcogenide, *Nat. Commun.*, 2018, **9**, 919.
15 M. Yoshida, T. Iizuka, Y. Saito, M. Onga, R. Suzuki, Y. Zhang, Y. Iwasa and S. Shimizu, Gate-optimized thermoelectric power factor in ultrathin WSe2 single crystals, *Nano Lett.*, 2016, **16**, 2061–2065.
16 K. Hippalgaonkar, Y. Wang, Y. Ye, D. Y. Qiu, H. Zhu, Y. Wang, J. Moore, S. G. Louie and X. Zhang, High thermoelectric power factor in two-dimensional crystals of Mo S 2, *Phys. Rev. B*, 2017, **95**, 115407.
17 M. Park, S. J. Hong, K. H. Kim, H. Kang, M. Lee, D. H. Jeong, Y. W. Park and B. H. Kim, Electrical and thermoelectric transport by variable range hopping in reduced graphene oxide, *Appl. Phys. Lett.*, 2017, **111**, 173103.

18 J. Kim, S. Youn, J. Bang, H. Moon, W. Jang, J. W. Roh, D. H. Kim, J. Chang and W. Lee, Experimental verification of semimetallic band structure in PtSe2 via thermoelectric power measurements, *Appl. Phys. Lett.*, 2022, **120**, 043103.
19 H. Moon, J. Bang, S. Hong, G. Kim, J. W. Roh, J. Kim and W. Lee, Strong thermopower enhancement and tunable power factor via semimetal to semiconductor transition in a transition-metal dichalcogenide, *ACS Nano*, 2019, **13**, 13317–13324.
20 W. Wang, B. Wang, Z. Gao, G. Tang, W. Lei, X. Zheng, H. Li, X. Ming and C. Autieri, Charge density wave instability and pressure-induced superconductivity in bulk 1 T-Nb S 2, *Phys. Rev. B*, 2020, **102**, 155115.
21 I. Naik, *Comparative Study between 2H-NbSe2 and 2H-TaSe2: Superconductivity and Charge Density Wave*, 2015.
22 I. Guillamon, H. Suderow, F. Guinea and S. Vieira, Intrinsic atomic-scale modulations of the superconducting gap of 2 H-NbSe 2, *Phys. Rev. B: Condens. Matter Mater. Phys.*, 2008, **77**, 134505.
23 R. Sooryakumar and M. Klein, Raman scattering by superconducting-gap excitations and their coupling to charge-density waves, *Phys. Rev. Lett.*, 1980, **45**, 660.
24 J. Shi, M. Hong, Z. Zhang, Q. Ji and Y. Zhang, Physical properties and potential applications of two-dimensional metallic transition metal dichalcogenides, *Coord. Chem. Rev.*, 2018, **376**, 1–19.
25 S. Zhao, T. Hotta, T. Koretsune, K. Watanabe, T. Taniguchi, K. Sugawara, T. Takahashi, H. Shinohara and R. Kitaura, Two-dimensional metallic NbS2: growth, optical identification and transport properties, *2D Mater.*, 2016, **3**, 025027.
26 P. Wang, Y. Huan, P. Yang, M. Cheng, J. Shi and Y. Zhang, Controlled syntheses and multifunctional applications of two-dimensional metallic transition metal dichalcogenides, *Acc. Mater. Res.*, 2021, **2**, 751–763.
27 J. Kim, S. Lee, Y. M. Brovman, P. Kim and W. Lee, Diameter-dependent thermoelectric figure of merit in single-crystalline Bi nanowires, *Nanoscale*, 2015, **7**, 5053–5059.
28 H. Moon, J. Kim, J. Bang, S. Hong, S. Youn, H. Shin, J. W. Roh, W. Shim and W. Lee, Semimetallic features in thermoelectric transport properties of 2H–3R phase niobium diselenide, *Nano Energy*, 2020, **78**, 105197.
29 G. Kresse and J. Furthmüller, Efficient iterative schemes for ab initio total-energy calculations using a plane-wave basis set, *Phys. Rev. B: Condens. Matter Mater. Phys.*, 1996, **54**, 11169.
30 P. E. Blöchl, Projector augmented-wave method, *Phys. Rev. B: Condens. Matter Mater. Phys.*, 1994, **50**, 17953.
31 J. P. Perdew, K. Burke and M. Ernzerhof, Generalized gradient approximation made simple, *Phys. Rev. Lett.*, 1996, **77**, 3865.
32 L. Lain, A. Torre, J. Karwowski and C. Valdemoro, Matrix elements of the third-order spin-adapted reduced Hamiltonian, *Phys. Rev. A*, 1988, **38**, 2721.
33 G. K. Madsen, J. Carrete and M. J. Verstraete, BoltzTraP2, a program for interpolating band structures and calculating semi-classical transport coefficients, *Comput. Phys. Commun.*, 2018, **231**, 140–145.
34 R. Euwema, D. Stukel, T. Collins, J. DeWitt and D. Shankland, Crystalline interpolation with applications to Brillouin-zone averages and energy-band interpolation, *Phys. Rev.*, 1969, **178**, 1419.
35 D. Shankland, Fourier transformation by smooth interpolation, *Int. J. Quantum Chem.*, 1971, **5**, 497–500.
36 D. Koelling and J. Wood, On the interpolation of eigenvalues and a resultant integration scheme, *J. Comput. Phys.*, 1986, **67**, 253–262.
37 M. Jiang, H. Xing, L. Zhang, L. Han, K. Zhang, C. Yao, D. Wang, X. Wang, S. Lan and X. Lv, Fast Switching of Bolometric and Self–Powered Effects in 2H–NbSe2 for High–Efficiency Low–Energy Photon Harvesting, *Adv. Opt. Mater.*, 2023, **11**, 2300074.
38 X. Zhu, Y. Guo, H. Cheng, J. Dai, X. An, J. Zhao, K. Tian, S. Wei, X. Cheng Zeng, C. Wu and Y. Xie, Signature of coexistence of superconductivity and ferromagnetism in two-dimensional NbSe2 triggered by surface molecular adsorption, *Nat. Commun.*, 2016, **7**, 11210.
39 Z. Li, X. Xi, B. Ding, H. Li, E. Liu, Y. Yao and W. Wang, Thermodynamics and kinetics synergy for controlled synthesis of 2D van der Waals single-crystal NbSe2 via modified chemical vapor transport, *Cryst. Growth Des.*, 2019, **20**, 706–712.
40 Y.-C. Zou, Z.-G. Chen, E. Zhang, F. Xiu, S. Matsumura, L. Yang, M. Hong and J. Zou, Superconductivity and magnetotransport of single-crystalline NbSe 2 nanoplates grown by chemical vapour deposition, *Nanoscale*, 2017, **9**, 16591–16595.
41 E. Hitz, J. Wan, A. Patel, Y. Xu, L. Meshi, J. Dai, Y. Chen, A. Lu, A. V. Davydov and L. Hu, Electrochemical intercalation of lithium ions into NbSe2 nanosheets, *ACS Appl. Mater. Interfaces*, 2016, **8**, 11390–11395.
42 S. Youn, J. Kim, H. Lee, D. H. Kim, J. Bang and W. Lee, Strong anisotropic transport properties of quasi-one-dimensional ZrTe3 nanoribbons, *Nano Energy*, 2024, **127**, 109771.
43 T. Zhu, P. M. Litwin, M. G. Rosul, D. Jessup, M. S. Akhanda, F. F. Tonni, S. Krylyuk, A. V. Davydov, P. Reinke, S. J. McDonnell and M. Zebarjadi, Transport properties of few-layer NbSe2: From electronic structure to thermoelectric properties, *Mater. Today Phys.*, 2022, **27**, 100789.
44 H. N. S. Lee, H. McKinzie, D. S. Tannhauser and A. Wold, The Low–Temperature Transport Properties of NbSe2, *J. Appl. Phys.*, 1969, **40**, 602–604.
45 K. S. Novoselov, D. Jiang, F. Schedin, T. J. Booth, V. V. Khotkevich, S. V. Morozov and A. K. Geim, Two-dimensional atomic crystals, *Proc. Natl. Acad. Sci. U. S. A.*, 2005, **102**, 10451–10453.
46 S. Youn, J. Kim, H. Moon, J.-K. Kim, J. Jang, J. Chang, T. Lee, K. Kang and W. Lee, Enhanced Thermoelectric Power Factor in Carrier-Type-Controlled Platinum Diselenide Nanosheets by Molecular Charge-Transfer Doping, *Small*, 2022, **18**, 2200818.

47 A. Boukai, K. Xu and J. R. Heath, Size-dependent transport and thermoelectric properties of individual polycrystalline bismuth nanowires, *Adv. Mater.*, 2006, **18**, 864–869.
48 A. Harzheim, C. Evangeli, O. V. Kolosov and P. Gehring, Direct mapping of local Seebeck coefficient in 2D material nanostructures via scanning thermal gate microscopy, *2D Mater.*, 2020, **7**, 041004.
49 K. Synnatschke, P. A. Cieslik, A. Harvey, A. Castellanos-Gomez, T. Tian, C.-J. Shih, A. Chernikov, E. J. Santos, J. N. Coleman and C. Backes, Length-and thickness-dependent optical response of liquid-exfoliated transition metal dichalcogenides, *Chem. Mater.*, 2019, **31**, 10049–10062.
50 Y. Zhang, H. Li, H. Wang, H. Xie, R. Liu, S.-L. Zhang and Z.-J. Qiu, Thickness considerations of two-dimensional layered semiconductors for transistor applications, *Sci. Rep.*, 2016, **6**, 29615.
51 X. Ni, H. Li and J.-L. Brédas, Organic self-assembled monolayers on superconducting NbSe2: interfacial electronic structure and energetics, *J. Phys.: Condens. Matter*, 2022, **34**, 294003.
52 S. Naik, G. K. Pradhan, S. G. Bhat, B. C. Behera, P. S. A. Kumar, S. L. Samal and D. Samal, The effect of Sn intercalation on the superconducting properties of 2HNbSe2, *Physica C*, 2019, **561**, 18–23.
53 S. Kim and Y.-W. Son, Quasiparticle energy bands and Fermi surfaces of monolayer ${\mathrm{NbSe}}_{2}$, *Phys. Rev. B*, 2017, **96**, 155439.
54 H. Luo, J. Strychalska-Nowak, J. Li, J. Tao, T. Klimczuk and R. J. Cava, S-Shaped Suppression of the Superconducting Transition Temperature in Cu-Intercalated NbSe2, *Chem. Mater.*, 2017, **29**, 3704–3712.
55 X. Xi, L. Zhao, Z. Wang, H. Berger, L. Forró, J. Shan and K. F. Mak, Strongly enhanced charge-density-wave order in monolayer NbSe2, *Nat. Nanotechnol.*, 2015, **10**, 765–769.
56 J.Á Silva-Guillén, P. Ordejón, F. Guinea and E. Canadell, Electronic structure of 2H-NbSe2 single-layers in the CDW state, *2D Mater.*, 2016, **3**, 035028.
57 Y. Wang, Y.-J. Hu, B. Bocklund, S.-L. Shang, B.-C. Zhou, Z.-K. Liu and L.-Q. Chen, First-principles thermodynamic theory of Seebeck coefficients, *Phys. Rev. B*, 2018, **98**, 224101.
58 I. Naik and A. K. Rastogi, Transport properties of 2H-NbSe2: Effect of Ga-intercalation, *Phys. B*, 2010, **405**, 955–957.
59 C. Zhang, S. Qiao, H. Xiao and T. Hu, Anisotropy of 2H-NbSe2 in the superconducting and charge density wave states, *Chin. Phys. B*, 2023, **32**, 047201.
60 S. Wang, X. Hou, P. Dong, Q. Dong, H. Shi, L. Ju, X. Hu, X. Hu, Z. Liu and T. Han, Weak dimensionality dependence of charge density wave transition in 2H-NbSe2, *Appl. Phys. Lett.*, 2023, **123**, 153505.
61 K. Iwaya, T. Hanaguri, A. Koizumi, K. Takaki, A. Maeda and K. Kitazawa, Electronic state of NbSe2 investigated by STM/STS, *Phys. B*, 2003, **329**, 1598–1599.
62 W. Hong-Tao, L. Lin-Jun, Y. De-Shu, C. Xin-Hong and X. Zhu-An, Effect of Te doping on superconductivity and charge-density wave in dichalcogenides 2H-NbSe2-xTex (x= 0, 0.1, 0.2), *Chin. Phys.*, 2007, **16**, 2471.
63 K. Cho, M. Kończykowski, S. Teknowijoyo, M. A. Tanatar, J. Guss, P. Gartin, J. Wilde, A. Kreyssig, R. McQueeney and A. I. Goldman, Using controlled disorder to probe the interplay between charge order and superconductivity in NbSe2, *Nat. Commun.*, 2018, **9**, 2796.
64 L. Li, J. Shen, Z. Xu and H. Wang, Magnetoresistance and hall effect of two-dimensional 2 H-NbSe 2, *Int. J. Mod. Phys. B*, 2005, **19**, 275–279.
65 X. Xi, Z. Wang, W. Zhao, J.-H. Park, K. T. Law, H. Berger, L. Forró, J. Shan and K. F. Mak, Ising pairing in superconducting NbSe2 atomic layers, *Nat. Phys.*, 2016, **12**, 139–143.
66 E. Khestanova, J. Birkbeck, M. Zhu, Y. Cao, G. L. Yu, D. Ghazaryan, J. Yin, H. Berger, L. Forró, T. Taniguchi, K. Watanabe, R. V. Gorbachev, A. Mishchenko, A. K. Geim and I. V. Grigorieva, Unusual Suppression of the Superconducting Energy Gap and Critical Temperature in Atomically Thin NbSe2, *Nano Lett.*, 2018, **18**, 2623–2629.
67 H. Lin, Q. Zhu, D. Shu, D. Lin, J. Xu, X. Huang, W. Shi, X. Xi, J. Wang and L. Gao, Growth of environmentally stable transition metal selenide films, *Nat. Mater.*, 2019, **18**, 602–607.
68 H. Wang, X. Huang, J. Lin, J. Cui, Y. Chen, C. Zhu, F. Liu, Q. Zeng, J. Zhou and P. Yu, High-quality monolayer superconductor NbSe2 grown by chemical vapour deposition, *Nat. Commun.*, 2017, **8**, 394.
69 N. E. Staley, J. Wu, P. Eklund, Y. Liu, L. Li and Z. Xu, Electric field effect on superconductivity in atomically thin flakes of NbSe 2, *Phys. Rev. B: Condens. Matter Mater. Phys.*, 2009, **80**, 184505.